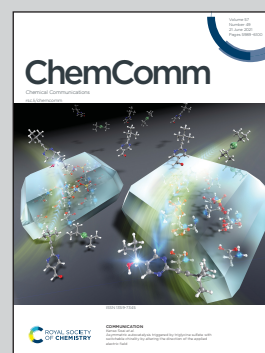


Showcasing research from Prof. Hiroto Nishihara's group and Mr Yuichiro Hayasaka, Tohoku University, Japan, collaborated with Dr Varisara Deerattrakul, National Nanotechnology Center, Thailand; Dr Jun Maruyama, Osaka Research Institute of Industrial Science and Technology, Japan; Prof. Kazuhide Kamiya's group, Osaka University, Japan; Prof. Fumito Tani's group, Kyushu University, Japan.

Force-responsive ordered carbonaceous frameworks synthesized from Ni-porphyrin

The force-responsive ordered carbonaceous frameworks have been synthesized for the first time. The mechanically flexible framework will open up new applications such as a new type of switching material and a force-responsive electrocatalyst.

As featured in:



See Hiroto Nishihara *et al.*, *Chem. Commun.*, 2021, **57**, 6007.


 Cite this: *Chem. Commun.*, 2021, 57, 6007

 Received 25th March 2021,
 Accepted 18th May 2021

DOI: 10.1039/d1cc01618k

rsc.li/chemcomm

Force-responsive ordered carbonaceous frameworks synthesized from Ni-porphyrin†

 Koki Chida,^a Takeharu Yoshii,^a Kazuma Takahashi,^a Masanori Yamamoto,^a Kazuya Kanamaru,^a Mao Ohwada,^a Varisara Deerattrakul,^b Jun Maruyama,^c Kazuhide Kamiya,^{d,e} Yuichiro Hayasaka,^f Masataka Inoue,^g Fumito Tani^g and Hiroto Nishihara^{ib,*ah}

Force-responsive ordered carbonaceous frameworks (OCFs) are synthesized for the first time. Carbonization of Ni porphyrin monomers having eight polymerizable ethynyl groups yields OCFs with atomically dispersed divalent Ni species and developed micropores. The highest specific surface area (673 m² g⁻¹) among the OCFs has been achieved. The OCFs thus synthesized comprise non-stacked graphene sheets, affording a unique mechanical flexibility that enables force-driven reversible phase transition.

Nanoporous carbon materials are used in various fields, such as electrodes, adsorbents, and catalyst supports, due to their superior thermal and chemical stability and electrical conductivity.¹ As new types of precursors for nanoporous carbon materials, organic nanoporous frameworks have recently attracted significant attention, such as metal organic frameworks (MOFs)² and covalent organic frameworks (COFs).³ One of the most distinct features of these precursors is the chemically defined ordered framework structures. However, their ordered structures are generally lost during the pyrolysis

process, resulting in amorphous carbonaceous materials.^{4–6} Thus, the molecular-level structure control of nanoporous carbon materials has remained a challenging target.

Our group has discovered that Ni porphyrin dimer (Ni₂-CPD_{py}) is an exceptional precursor, which can preserve its ordered structure even after carbonization. The ordered carbonaceous frameworks (OCFs) thus obtained retain the porphyrin-derived Ni-N₄ coordination units and exhibit effective electrocatalysis for CO₂ conversion into CO.⁷ More recently, we have extended OCF precursors to Ni- or Fe-porphyrin monomers with ethynyl groups, which can be synthesized much more readily than Ni₂-CPD_{py}.^{8,9} OCFs have both advantages of MOFs and carbon materials, *i.e.*, chemically defined ordered structure, thermal/chemical stability, and electrical conductivity, towards a variety of applications such as electrocatalysis and gas separation/storage.^{10–12}

One of the interesting features of OCFs is that their frameworks are composed of non-stacked graphene sheets,^{7–9} which is analogous to nanoporous materials with single-graphene walls such as zeolite-templated carbon (ZTC)¹³ and graphene mesosponge (GMS).¹⁴ In this work, we shine a spotlight on the non-stacked graphene framework of OCFs. Single-graphene frameworks of ZTC and GMS make them extraordinarily flexible despite their small pore size (< 10 nm), and such an elastic property could afford new functions, such as force-driven reversible phase transition.¹⁵ However, unlike ZTC and GMS, the previously reported OCFs were not highly porous enough to exhibit elastic deformation by external force. Herein, we synthesize force-responsive OCFs for the first time. By introducing eight ethynyl groups in a porphyrin monomer, the porosity of OCFs is remarkably enhanced and force-driven phase transition is successfully demonstrated. The mechanical flexibility of OCFs will open up new applications such as force-responsive electrocatalysis and on-off switching materials like a cytochrome complex.¹⁶

As a precursor of new OCFs, a Ni porphyrin monomer having eight ethynyl groups ([5,10,15,20-tetrakis(3,5-diethynylphenyl)porphinato] nickel(II)), which is denoted as Ni-P_{8e} (Fig. 1a),

^a Institute of Multidisciplinary Research for Advanced Materials, Tohoku University, 2-1-1 Katahira, Aoba-ku, Sendai, Miyagi, 980-8577, Japan.

E-mail: hirotomo.nishihara.b1@tohoku.ac.jp

^b National Nanotechnology Centre (NANOTEC), National Science and Technology Development Agency (NSTDA), Pathum Thani, 12120, Thailand
^c Research Division of Environmental Technology, Osaka Research Institute of Industrial Science and Technology, 1-6-50 Morinomiya, Joto-ku, Osaka, 536-8553, Japan

^d Graduate School of Engineering Science, Osaka University, 1-3 Machikaneyama, Toyonaka, Osaka, 560-8531, Japan

^e Research Centre for Solar Energy Chemistry, Osaka University, 1-3 Machikaneyama, Toyonaka, Osaka, 560-8531, Japan

^f The Electron Microscopy Centre, Tohoku University, 2-1-1 Katahira, Aoba, Sendai, Miyagi, 980-8577, Japan

^g Institute for Materials Chemistry and Engineering, Kyushu University, 744 Motoooka, Nishi-ku, Fukuoka 819-0395, Japan

^h Advanced Institute for Materials Research (WPI-AIMR), Tohoku University, 2-1-1 Katahira, Aoba-ku, Sendai, Miyagi, 980-8577, Japan

† Electronic supplementary information (ESI) available: Experimental details and additional characterization data. CCDC 2063651. For ESI and crystallographic data in CIF or other electronic format see DOI: 10.1039/d1cc01618k

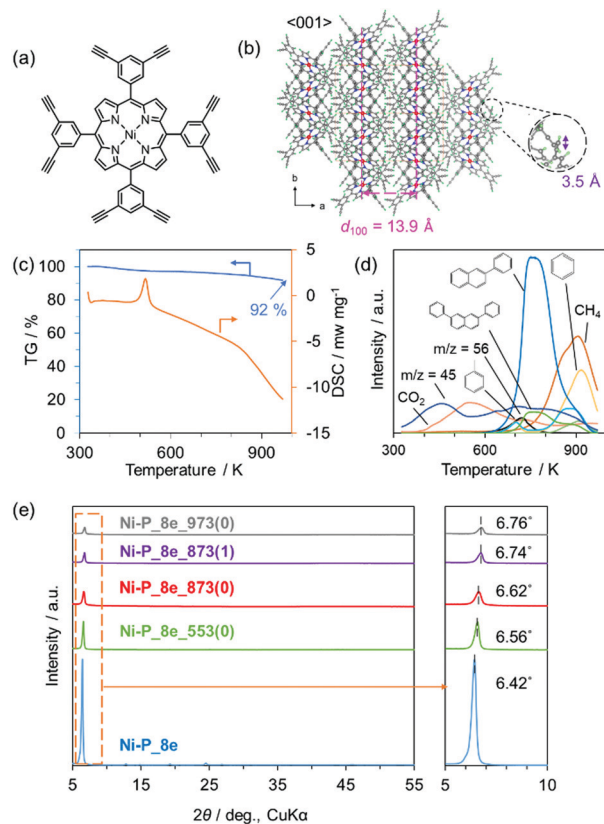


Fig. 1 (a and b) Structures of Ni-P_{8e}. (a) A single molecule and (b) packing structure (CCDC† 2063651). (c) TG–DSC and (d) MS results of Ni-P_{8e}. (e) PXRD patterns of Ni-P_{8e} and heat-treated samples.

was synthesized according to Scheme S1 (ESI†).^{17,18} Successful synthesis was confirmed by ¹H NMR (Fig. S1, ESI†), ¹³C NMR (Fig. S2, ESI†) and matrix-assisted laser desorption/ionization-time of flight-mass spectroscopies (Fig. S3, ESI†). The packing structure of Ni-P_{8e}, which is free from solvent molecules was solved by powder X-ray crystallography using the direct space method and Rietveld refinement (for details, see Fig. S4, ESI†).^{7–9}

As shown in Fig. 1b, the Ni-P_{8e} molecules are alternately arranged, while tilted at 90°. Notably, the distances between ethynyl groups are within the range of 5 Å (the shortest is 3.5 Å). It is known that the suitable distance between polymerizable groups in monomer molecules is less than 5 Å for the structure-preserving solid phase polymerization, or topochemical polymerization.¹⁹ Therefore, the crystal structure of Ni-P_{8e} is appropriate for the thermal polymerization, while keeping the molecular order. Prior to the pyrolysis, the thermal behaviour of Ni-P_{8e} was analysed using thermogravimetry–differential scanning calorimetry–mass spectroscopy (TG–DSC–MS; Fig. 1c and d). Significant weight loss was not observed in the TG curve, and a high yield (92%) can be obtained even after the heat treatment at 973 K, demonstrating the outstanding thermal stability of the precursor. The DSC curve exhibits a large exothermic peak at 520 K, suggesting that ethynyl groups are thermally polymerized. The enthalpy change calculated from the exothermic peak is 100 kJ per 1 mol of ethynyl groups,

which is much larger than the reported value (29 kJ mol^{−1}) for Ni porphyrin with two ethynyl groups (for details, see Table S1, ESI†).⁸ This result indicates that more efficient polymerization occurred in Ni-P_{8e}. Indeed, the disappearance of sp bonding due to thermal polymerization at 553 K was confirmed by ¹³C NMR (Fig. S5, ESI†).²⁰ When the temperature exceeds 600 K, aromatic compounds such as 2-phenylnaphthalene, benzene, and toluene are emitted, corresponding to slight weight loss (Fig. 1c), due to the thermal decomposition. In Raman measurement (Fig. S6, ESI†), multiple sharp peaks are shown in Ni-P_{8e}, and some of them are retained in the polymer prepared at 553 K. In contrast, the sample heat-treated at 973 K shows only broad G- and D-bands,²¹ indicating the formation of defective graphene sheets, which is also supported by X-ray photoelectron spectroscopy (XPS) analysis (Fig. S7, ESI†). Considering these results, ethynyl groups of Ni-P_{8e} are thermally polymerized at around 553 K without decomposition reactions, and then, the resulting polymer is turned into carbonaceous frameworks above 600 K.

Based on the above results, carbonized samples were prepared by a simple pyrolysis of Ni-P_{8e} at a heating rate of 10 K min^{−1} under a N₂ flow without any specific operations such as activation and acid washing. The carbonized samples are denoted as Ni-P_{8e}_X(Y): X and Y indicate heat treatment temperature (K) and holding time (h), respectively. The change of powder X-ray diffraction (PXRD) pattern of Ni-P_{8e} upon heating is summarized in Fig. 1e. Ni-P_{8e} shows a sharp peak at 6.42° from the (100) plane (Fig. 1b). The distinct peak is observed in the series of heat-treated samples. Unlike the carbonization of porphyrin with two ethynyl groups,⁹ the ordered structure is retained up to 973 K, indicating a significant thermal stability of Ni-P_{8e} because of the developed cross-linking network. It is noteworthy that all the carbonized samples do not show carbon 002 and 10 PXRD peaks at 26° and 44°, respectively (for details, see Fig. S8, ESI†). Thus, the carbonized samples do not contain graphene stacking structures nor widely developed graphene domains. These features are similar to the characteristic of ZTC, which is force-responsive metal-free microporous carbon.^{13,15} The scanning electron microscopy (SEM) image of Ni-P_{8e}_873(0) is shown in Fig. 2a. A plate-like crystal morphology of Ni-P_{8e} (Fig. S9a, ESI†) is well retained at 553 K (heat-polymerized polymer, Fig. S9b, ESI†) and at 873 K (carbonized sample, Fig. 2a).

Next, the state of Ni species is investigated. From PXRD patterns (Fig. S8, ESI†), there is no evident peaks corresponding to Ni metal or Ni oxide for Ni-P_{8e}_873(0) and Ni-P_{8e}_873(1). In Ni-P_{8e}_973(0), very weak peaks of Ni metal²² appear, indicating that Ni agglomeration starts to occur above 973 K. Transmission electron microscopy (TEM) also reveals no aggregation of Ni species in Ni-P_{8e}_873(0) (Fig. 2b), whereas Ni nanoparticles are found in Ni-P_{8e}_973(0) (Fig. S10, ESI†). A high-magnification image of Ni-P_{8e}_873(0) is obtained by high angle annular dark-field scanning transmission electron microscopy (HAADF-STEM), in which the position of heavy element (Ni) appears as bright contrast. Fig. 2c shows that Ni atoms are aligned with the periodicity of 1.3 nm, which is in

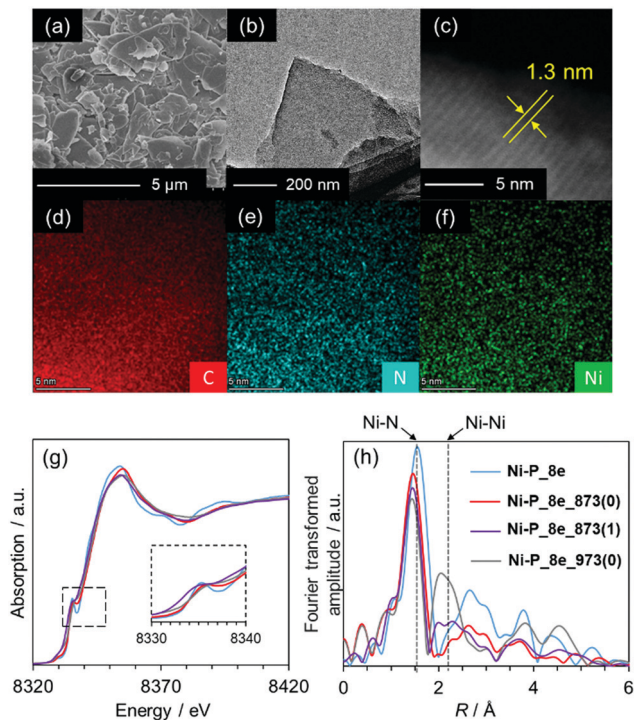


Fig. 2 (a) SEM, (b) TEM, (c) HAADF-STEM, and (d–f) EDS elemental mapping images of Ni-P_{8e}_873(0). (g) Ni-K edge XANES spectra and (h) RSFs of Ni-P_{8e} and the heat-treated samples.

good agreement with the d-spacing determined by the PXRD peak at 6.62° (Fig. 1e). The energy dispersive spectroscopy (EDS) elemental mapping images (Fig. 2d–f) indicate that C, N and Ni atoms are homogeneously dispersed throughout the material. The amounts of N and Ni in the carbonized sample are almost in accordance with those of Ni-P_{8e} (Table S2, ESI[†]).

To get insight into the local structure around Ni, X-ray absorption fine structure (XAFS) of the Ni-K edge was measured by synchrotron X-ray absorption spectroscopy. The shapes of the X-ray absorption near edge spectroscopy (XANES) spectra (Fig. 2g) are similar in the series of the samples derived from Ni-P_{8e}. The absorption edge energy of Ni-P_{8e} (8339 eV) is unchanged after carbonization, and thus, the Ni(II) state is retained after the pyrolysis. Additionally, a pre-edge peak of Ni-P_{8e} at 8336 eV, which is derived from the 1s to 4p_z transition,²³ also appears in the carbonized derivatives, suggesting the existence of planar Ni-N₄ units in the carbonaceous framework. As shown in radial structure function (RSF, Fig. 2h) calculated from the oscillation function (Fig. S11, ESI[†]) of extended X-ray absorption fine structure (EXAFS), all the samples exhibit a shell at 1.6 Å associated with the Ni-N bond. Only in the case of Ni-P_{8e}_973(0), a shell at 2.2 Å assigned to a Ni-Ni bond is observed (Fig. S12, ESI[†]). In addition, fitting a first coordination shell for the Ni-N bond suggests only a slight decrease of average coordination number with the heat treatment progress (Table S3, ESI[†]). These XAFS results demonstrate that the Ni-N₄ coordination structure of Ni-P_{8e} is thermally stable and maintained up to 873 K, and then, Ni species partly aggregated to form Ni nanoparticles when the temperature

reaches 973 K. The XAFS results are consistent with the above-mentioned PXRD and TEM results. The high thermal stability of the Ni-N₄ unit is also supported by no detection of pyrrole groups⁷ in TG–DSC–MS measurement (see Fig. 1d).

Fig. 3a displays N₂ adsorption/desorption isotherms of Ni-P_{8e} and its heat-treated derivatives. The specific surface areas calculated by the Brunauer–Emmett–Teller (BET) method (S_{BET}) and total pore volume (V_{total}) are summarized in Table S4 (ESI[†]). The S_{BET} of originally non-porous Ni-P_{8e} ($11 \text{ m}^2 \text{ g}^{-1}$) slightly increases by the thermal polymerization at 553 K ($55 \text{ m}^2 \text{ g}^{-1}$). By the carbonization at 873 K, the microporosity is remarkably developed. Ni-P_{8e}_873(1) shows the largest recorded S_{BET} ($673 \text{ m}^2 \text{ g}^{-1}$) in OCF materials reported thus far (see Table S4, ESI[†]). However, at 973 K, the S_{BET} drops to $267 \text{ m}^2 \text{ g}^{-1}$, probably due to the structure destruction caused by the aggregation of Ni species. Notably, pore size distributions of the OCFs calculated by the DFT method (Fig. 3b) indicate the formation of uniform-sized micropores, demonstrating the advantage of the crystalline precursor. The successful development of micropores can be ascribed to a large number of polymerizable ethynyl groups in Ni-P_{8e}. As reference, the carbonization behaviours of monomers with less number of ethynyl groups were compared: Ni and Fe porphyrins with two ethynyl groups, which were reported elsewhere^{8,9} and two new Ni porphyrins with two (7) and four (10) ethynyl groups (see Scheme S2 and Fig. S13–S17, ESI[†]). The ordered structures of 7 and 10 are lost at 873 K, as found in their PXRD patterns (Fig. S18, ESI[†]). Instead, a broad peak at 26° appears due to the stacking of graphene sheets. Thus, OCFs were not obtained from 7 and 10. The relation between S_{BET} of carbonized samples and the number of ethynyl groups in the monomers are summarized in Fig. S19 and Table S5 (ESI[†]). There is a general tendency in which S_{BET} increases with the number of ethynyl groups.

From the non-stacked graphene framework and the developed micropores, the OCFs derived from Ni-P_{8e} are expected to be mechanically flexible. Thus, the force-responsive property of Ni-P_{8e}_873(0) was investigated by methanol-vapour adsorption/desorption measurement with and without loading mechanical force using a closed chamber, which is equipped with a bellows-sealed linear feedthrough (Fig. S20, ESI[†]).^{14,15}

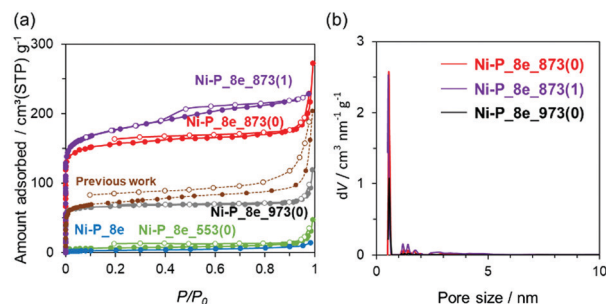


Fig. 3 (a) N₂ adsorption/desorption isotherms at 77 K of Ni-P_{8e} and the heat-treated samples with the previously reported OCF.⁸ (b) Pore size distribution of the carbonized samples calculated by the DFT method.

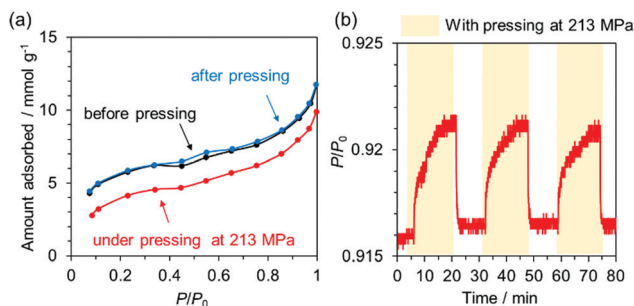


Fig. 4 (a) Methanol adsorption isotherms (298 K) of Ni-P_{8e}-873(0) before (black), under (red) and after (blue) the application of a mechanical force (213 MPa). (b) Fluctuation of methanol vapour pressure inside the chamber during applying/releasing a mechanical force to Ni-P_{8e}-873(0).

As demonstrated in Fig. 4a, the methanol adsorption amount is decreased by applying a mechanical force (213 MPa). When the force is released, the adsorption amount is completely recovered. These results indicate reversible nanopore contraction/recovery by mechanical force. Such force-responsive behaviour has not been reported in conventional activated carbons.¹⁴ The elasticity of Ni-P_{8e}-873(0) is further demonstrated by the force-driven methanol liquid-gas phase transition (Fig. 4b).¹⁵ Ni-P_{8e}-873(0) is placed in a closed chamber containing methanol vapour and the adsorption equilibrium is established at $P/P_0 = 0.916$. When a force (213 MPa) is applied to Ni-P_{8e}-873(0), the methanol vapour pressure is increased to $P/P_0 = 0.922$, indicating force-driven desorption of methanol, which was adsorbed on Ni-P_{8e}-873(0). When the force is removed, the vapour pressure decreases to $P/P_0 = 0.916$ because of the re-adsorption of methanol in recovered Ni-P_{8e}-873(0). Moreover, a good repeatability is demonstrated against pressing with 213 MPa three times. This phenomenon is also confirmed using ethanol as an adsorbate (Fig. S21, ESI†). Note that the change of P/P_0 caused by the dead-volume change is negligible compared to the result of Fig. 4b (Fig. S22, ESI†). Fig. 4 clearly indicates that the OCF functions as an elastic nanosponge. The mechanically soft OCFs are expected to be used for new applications such as force-responsive electrocatalysis.

In summary, a new type of OCF with mechanical flexibility has been synthesized by a simple carbonization of Ni porphyrin monomer with eight ethynyl groups. A large number of ethynyl groups in a monomer molecule is effective to develop microporosity, and the largest recorded S_{BET} ($673 \text{ m}^2 \text{ g}^{-1}$) is achieved in OCF materials reported thus far. The OCFs have uniform-sized micropores and the ordered framework containing single Ni atom sites with the Ni-N₄ coordination structure. Furthermore, the OCFs have a unique mechanical flexibility, and force-driven reversible phase transition has been demonstrated. These findings offer the opportunity to design new systems using flexible carbonaceous frameworks containing single metal atoms, paving the way for multiple applications of OCFs involving catalysts, adsorbents, and gas separation/storage.

This work was supported by JST CREST Grant no. JPMJCR18R3; the “Five-star Alliance” in “NJRC Mater. & Dev.”;

Japan Association for Chemical Innovation. The XAFS spectra were recorded at the BL01B1 and BL14B2 stations in SPring-8, Harima, Japan (Proposal no. 2020A1254 and 2020A1604, respectively). The authors acknowledge Prof. T. Kyotani for his advice, Prof. H. Kato for his kind support in Raman spectroscopy, Prof. Y. Nishina for his advice on catalysis, and Mr S. Yoshida for his kind support in ¹³C NMR measurements.

Conflicts of interest

There are no conflicts to declare.

Notes and references

- 1 B. Marinho, M. Ghislandi, E. Tkalya, C. E. Koning and G. de With, *Powder Technol.*, 2012, **221**, 351–358.
- 2 L. Pan, D. H. Olson, L. R. Ciemnomolonski, R. Heddy and J. Li, *Angew. Chem., Int. Ed.*, 2006, **45**, 616–619.
- 3 Z. Q. Luo, L. J. Liu, J. X. Ning, K. X. Lei, Y. Lu, F. J. Li and J. Chen, *Angew. Chem., Int. Ed.*, 2018, **57**, 9443–9446.
- 4 W. Chaikittisilp, K. Ariga and Y. Yamauchi, *J. Mater. Chem. A*, 2013, **1**, 14–19.
- 5 H. L. Jiang, B. Liu, Y. Q. Lan, K. Kuratani, T. Akita, H. Shioyama, F. Q. Zong and Q. Xu, *J. Am. Chem. Soc.*, 2011, **133**, 11854–11857.
- 6 K. Nakatsuka, T. Yoshii, Y. Kuwahara, K. Mori and H. Yamashita, *Chem. – Eur. J.*, 2018, **24**, 898–905.
- 7 H. Nishihara, T. Hirota, K. Matsuura, M. Ohwada, N. Hoshino, T. Akutagawa, T. Higuchi, H. Jinnai, Y. Koseki, H. Kasai, Y. Matsuo, J. Maruyama, Y. Hayasaka, H. Konaka, Y. Yamada, S. Yamaguchi, K. Kamiya, T. Kamimura, H. Nobukuni and F. Tani, *Nat. Commun.*, 2017, **8**, 109.
- 8 H. Nishihara, K. Matsuura, M. Ohwada, M. Yamamoto, Y. Matsuo, J. Maruyama, Y. Hayasaka, S. Yamaguchi, K. Kamiya, H. Konaka, M. Inoue and F. Tani, *Chem. Lett.*, 2020, **49**, 619–623.
- 9 M. Yamamoto, K. Takahashi, M. Ohwada, W. Yuxin, K. Iwase, Y. Hayasaka, H. Konaka, H. Cove, D. D. Tommaso, K. Kamiya, J. Maruyama, F. Tani and H. Nishihara, *Catal. Today*, 2021, **364**, 164–171.
- 10 S. L. Hou, J. Dong, X. L. Jiang, Z. H. Jiao and B. Zhao, *Angew. Chem., Int. Ed.*, 2019, **58**, 577–581.
- 11 J. R. Li, R. J. Kuppler and H. C. Zhou, *Chem. Soc. Rev.*, 2009, **38**, 1477–1504.
- 12 S. R. Venna, M. Lartey, T. Li, A. Spore, S. Kumar, H. B. Nulwala, D. R. Luebke, N. L. Rosi and E. Albenze, *J. Mater. Chem. A*, 2015, **3**, 5014–5022.
- 13 H. Nishihara and T. Kyotani, *Chem. Commun.*, 2018, **54**, 5648–5673.
- 14 H. Nishihara, T. Simura, S. Kobayashi, K. Nomura, R. Berenguer, M. Ito, M. Uchimura, H. Iden, K. Arihara, A. Ohma, Y. Hayasaka and T. Kyotani, *Adv. Funct. Mater.*, 2016, **26**, 6418–6427.
- 15 K. Nomura, H. Nishihara, M. Yamamoto, A. Gabe, M. Ito, M. Uchimura, Y. Nishina, H. Tanaka, M. T. Miyahara and T. Kyotani, *Nat. Commun.*, 2019, **10**, 10.
- 16 H. Z. Wang, T. Matsuo, S. Nagao and S. Hirota, *Org. Biomol. Chem.*, 2011, **9**, 47666–47669.
- 17 D. D. Yao, X. Zhang, O. Mongin, F. Paul and C. O. Paul-Roth, *Chem. – Eur. J.*, 2016, **22**, 5583–5597.
- 18 J. D. Megiatto, R. Spencer and D. I. Schuster, *J. Mater. Chem.*, 2011, **21**, 1544–1550.
- 19 A. Matsumoto, *Polym. J.*, 2003, **35**, 93–121.
- 20 F. McCoy, D. C. Apperley, B. Variano, H. Sussman, D. Loeven, P. Boyd and R. K. Malcolm, *Int. J. Pharm.*, 2018, **548**, 689–697.
- 21 M. J. Matthews, M. A. Pimenta, G. Dresselhaus, M. S. Dresselhaus and M. Endo, *Phys. Rev. B: Condens. Matter Mater. Phys.*, 1999, **59**, R6585–R6588.
- 22 Y. H. Lv, Z. Xin, X. Meng, M. Tao and Z. C. Bian, *Microporous Mesoporous Mater.*, 2018, **262**, 89–97.
- 23 J. T. Miller, R. B. Fisher, A. M. J. van der Eerden and D. C. Koningsberger, *Energy Fuels*, 1999, **13**, 719–727.